An Optimized Switching Strategy for Quick Dynamic Torque Control in DTC Hysteresis-Based Induction Machines

Auzani Jidin, *Student Member, IEEE,* Nik Rumzi Nik Idris, *Senior Member, IEEE,* Abdul Halim Mohamed Yatim, *Senior Member, IEEE,* Tole Sutikno, *Student Member, IEEE,* Malik E. Elbuluk, *Senior Member, IEEE*

***Abstract*—A dynamic overmodulation strategy for fast dynamic torque control in direct torque control (DTC)-hysteresis based induction machine is proposed. The fastest dynamic torque response with six-step mode can be achieved in the proposed method by switching only the most optimized voltage vector that produce the largest tangential component to the circular flux locus. The paper also discusses the performance of dynamic torque control in basic DTC in order to justify on how the proposed selected voltage vector results in excellent dynamic torque performance. The main benefit of the proposed method is its simplicity since it only requires a minor modification to the conventional DTC hysteresis-based structure and does not require the space vector modulator. To verify the feasibility of the proposed dynamic overmodulation strategy simulation and experimentation as well as comparison with the conventional DTC scheme are carried out. The results showed the significant improvement in the dynamic torque response when compared to the conventional DTC hysteresis-based method.**

***Index Terms*—Dynamic overmodulation, direct torque control (DTC), induction machine, hysteresis controller, torque control.**

I. Introduction

OVER the past years, Direct Torque Control (DTC) scheme for induction motor drives has received enormous attention in industrial motor drive applications. The main reason for its popularity is due to its simple structure, especially when compared with field-oriented control (FOC) scheme, which was introduced a decade earlier. Since DTC was first introduced, several variations to its original structure (which we referred to as DTC hysteresis-based) [1] were proposed to overcome the inherent disadvantages in any hysteresis-based controller such as, variable switching frequency, high sampling requirement for digital implementation and high torque ripple [2]-[11]. Recently, predictive control strategy has found applications in motor drives [12]-[21]. Predictive control applied to DTC has gain considerable amount of attention particularly due to its ability to reduce the torque ripple and as well as switching frequency [8]-[10],[21]. In particular model predictive control (MPC) which was applied in [8] and [9] uses the hysteresis comparators but with the switching table replaced with online optimization algorithm. However, the application of MPC during a large step change in torque demand will result in significant computational burden whereas, as will be shown later in this paper, a simplified method can be used. Furthermore the use of MPC during large step change in torque command does not guarantee fastest torque response.

The most popular variation of DTC of induction motor drives is the one that is based on space vector modulation (SVM), which normally referred to as DTC-SVM [22]-[31]. The major difference between DTC hysteresis-based and DTC-SVM is the way the stator voltage is generated. In DTC hysteresis-based the applied stator voltage depends on voltage vectors, which are selected from a look-up table. The selections are based on the requirement of the torque and flux demand obtained from the hysteresis comparators. On the other hand, in DTC-SVM, a stator voltage reference is calculated or generated within a sampling period, which is then synthesized using the space vector modulator. The stator voltage reference vector is calculated based on the requirement of torque and flux demands. Due to the regular sampling in SVM, the DTC-SVM produces constant switching frequency as opposed to the variable switching frequency in hysteresis-based DTC however, at the expense of more complex implementation. Various methods to estimate the voltage reference vector, had been reported; these include the use of proportional-integral current controller [23], stator flux vector error [24] [25], proportional-integral torque and flux controllers [26]-[28], predictive and dead-beat controllers [29]-[31]. During large torque demand, it is inevitable that this

Manuscript received March 23, 2010. (Write the date on which you submitted your paper for review.) Accepted for publication September 10, 2010 (Write the date your paper was accepted).

Auzani Jidin is with Department of Power Electronics and Drives, Faculty of Electrical Engineering, Universiti Teknikal Malaysia Melaka, Hang Tuah Jaya, 76100 Durian Tunggal, Malacca, Malaysia (e-mail: auzani@utem.edu.my).

Nik Rumzi Nik Idris and Abdul Halim M. Yatim are with Department of Energy Conversion, Faculty of Electrical Engineering, Universiti Teknologi Malaysia, 81310 UTM, Johor, Malaysia (email: nikrumzi@ieee.org).

Tole Sutikno is with Department of Electrical Engineering, Faculty of Industrial Technology, Universitas Ahmad Dahlan, Jln. Prof. Soepomo, Janturan, Yogyakarta, Indonesia (email: tole@ee.uad.ac.id).

M. E. Elbuluk is with the Department of Electrical and Computer Engineering, University of Akron, Akron, OH 44325-3904 USA (e-mail: melbuluk@uakron.edu).

reference exceeds the voltage vector limits enclosed by the hexagonal boundary. Under this condition, the SVM has to be operated in what is termed as dynamic overmodulation mode. The voltage reference vector has to be modified such that it will lie on the hexagonal boundary. Several methods [29][30][32][33] have been proposed and to some extent, these methods have managed to minimize the voltage vector error as well as obtained a fast torque response, however the majority of them do not guarantee the fastest torque response.

In hysteresis-based DTC, during large torque demand, the torque hysteresis comparator will give an output that demands the selection of voltage vector to increase the torque. At the same time, a flux hysteresis comparator will regulate the flux to achieve a circular flux path. This circular flux path however, does not correspond to the fastest torque demand. In other words, the basic method that is used to select the voltage vectors in hysteresis-based DTC will not guarantee the fastest torque response. A minor modification to the voltage vector selection needs to be performed to ensure fastest torque response during this condition.

In this paper, a simple DTC hysteresis-based with fastest dynamic torque response is presented. The voltage vector used in this proposed dynamic overmodulation is similar with that proposed in [31] and [34]; however [31] uses a DTC-SVM with complex predictive stator flux control structure while in [34] the stator current contains lower harmonic contents at any operating condition due to the hexagonal shape of the stator flux locus. In this paper, the optimized voltage vector to produce fast dynamic response corresponds to the voltage vector that produces the largest tangential flux component is selected. The selection of the optimized voltage vector can be simply done by modifying the flux error status before it is being fed to the look-up table. In this way, the fastest dynamic torque control with six-step operation is achieved and the simple structure of DTC hysteresis-based is retained without the need of SVM. In section II of the paper, the basic principle of DTC is briefly discussed. Section III discusses the previous proposed methods of dynamic overmodulation. The dynamic overmodulation operation in basic DTC hysteresis-based and the proposed dynamic overmodulation method for DTC hysteresis-based are also discussed. Section IV presents the simulation and experimental results of the proposed method. Finally conclusion is given in Section V.

II. Principle of DTC

The behavior of induction machine in DTC drives can be described in terms of space vectors by the following equations written in stator stationary reference frame.

$$\mathbf{v_s} = \mathrm{r_s}\,\mathbf{i_s} + \frac{\mathrm{d}\,\mathbf{\Psi_s}}{\mathrm{dt}} \tag{1}$$

$$0 = \mathrm{r_r}\,\mathbf{i_r} - \mathrm{j}\omega_\mathrm{r}\,\mathbf{\Psi_r} + \frac{\mathrm{d}\,\mathbf{\Psi_r}}{\mathrm{dt}} \tag{2}$$

$$\mathbf{\Psi_s} = \mathrm{L_s}\,\mathbf{i_s} + \mathrm{L_m}\,\mathbf{i_r} \tag{3}$$

$$\mathbf{\Psi_r} = \mathrm{L_r}\,\mathbf{i_r} + \mathrm{L_m}\,\mathbf{i_s} \tag{4}$$

$$\mathrm{T_e} = \frac{3}{2}\mathrm{P}\,|\,\mathbf{\Psi_s}\,|\,|\mathbf{i_s}\,|\sin\delta \tag{5}$$

where P is the number of pole pairs, ω_r is the rotor electric angular speed in rad./s, L_s, L_r and L_m are the motor inductances and δ is the angle between the stator flux linkage and stator current space vectors. Based on (1) the d^s- and q^s-axis stator flux in a stationary reference frame can be written as,

$$\Psi_{s,d}{}^{s} = \int (v_{s,d}{}^{s} - i_{s,d}{}^{s} r_s)\ \mathrm{dt} \tag{6a}$$

$$\Psi_{s,q}{}^{s} = \int (v_{s,q}{}^{s} - i_{s,q}{}^{s} r_s)\ dt \tag{6b}$$

In terms of switching states S_a, S_b, and S_c (can be either 0 or 1) the voltage vectors in (6) are given by

$$v_{s,d}{}^{s} = \frac{1}{3} V_{dc}(2S_a - S_b - S_c) \tag{7a}$$

$$v_{s,q}{}^{s} = \frac{1}{\sqrt{3}} V_{dc}(S_b - S_c) \tag{7b}$$

The electromagnetic torque given in (5) can be rewritten in d^s-q^s coordinates as

$$\mathrm{T_e} = \frac{3}{2}\mathrm{P}(\Psi_{s,d}{}^{s} i_{s,q}{}^{s} - \Psi_{s,q}{}^{s} i_{s,d}{}^{s}) \tag{8}$$

Fig. 1 shows the structure of DTC hysteresis-based as initially proposed by [1]. The output stator voltage is applied based on the selection of the switching states (S_a, S_b, S_c) obtained from the look-up table. These switching states are selected based on the requirement as to whether the torque and the stator flux need to be increased or decreased and also on the stator flux position. The decisions as to whether the torque and/or the flux need to be increased or otherwise comes from the three-level and two-level hysteresis comparators for the torque and stator flux, respectively. The outputs from the torque and flux hysteresis comparators are labeled as T_{stat}

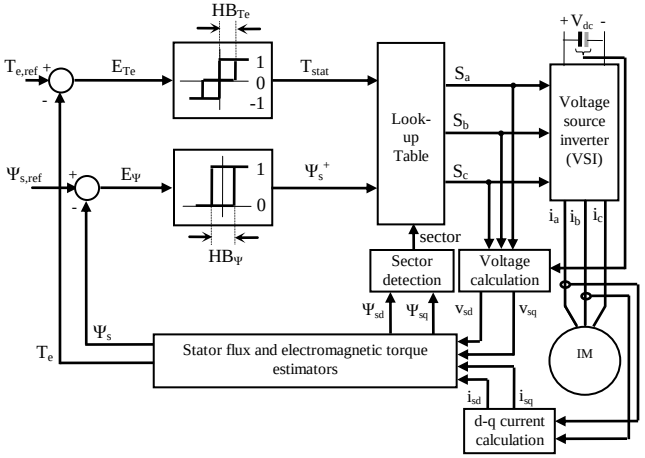

Fig. 1. Structure of basic DTC-hysteresis based induction machine.

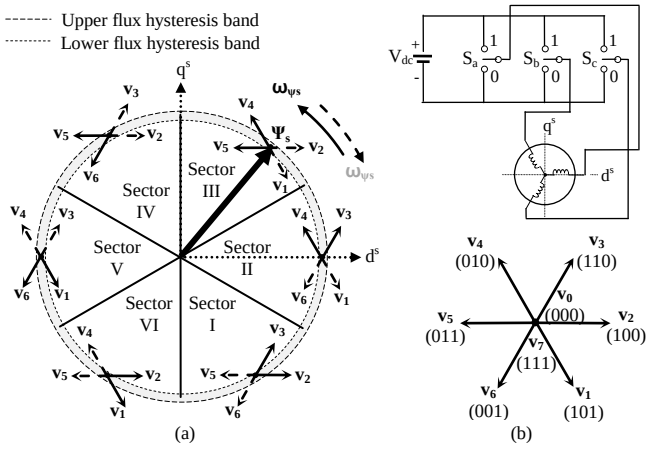

Fig. 2. Selection of the optimum inverter output voltage vectors (a) Each sector indicates the appropriate voltage vectors. (b) Eight possible switches configuration in the three-phase VSI.

TABLE I
LOOK-UP TABLE (VOLTAGE VECTOR SELECTION)

Stator flux error status, Ψ_s^+	Torque error status, T_{stat}	Sector I	Sector II	Sector III	Sector IV	Sector V	Sector VI
1	1	$\mathbf{v_2}$ (100)	$\mathbf{v_3}$ (110)	$\mathbf{v_4}$ (010)	$\mathbf{v_5}$ (011)	$\mathbf{v_6}$ (001)	$\mathbf{v_1}$ (101)
	0	$\mathbf{v_0}$ (000)	$\mathbf{v_7}$ (111)	$\mathbf{v_0}$ (000)	$\mathbf{v_7}$ (111)	$\mathbf{v_0}$ (000)	$\mathbf{v_7}$ (111)
	-1	$\mathbf{v_6}$ (001)	$\mathbf{v_1}$ (101)	$\mathbf{v_2}$ (100)	$\mathbf{v_3}$ (110)	$\mathbf{v_4}$ (010)	$\mathbf{v_5}$ (011)
0	1	$\mathbf{v_3}$ (110)	$\mathbf{v_4}$ (010)	$\mathbf{v_5}$ (011)	$\mathbf{v_6}$ (001)	$\mathbf{v_1}$ (101)	$\mathbf{v_2}$ (100)
	0	$\mathbf{v_7}$ (111)	$\mathbf{v_0}$ (000)	$\mathbf{v_7}$ (111)	$\mathbf{v_0}$ (000)	$\mathbf{v_7}$ (111)	$\mathbf{v_0}$ (000)
	-1	$\mathbf{v_5}$ (011)	$\mathbf{v_6}$ (001)	$\mathbf{v_1}$ (101)	$\mathbf{v_2}$ (100)	$\mathbf{v_3}$ (110)	$\mathbf{v_4}$ (101)

III. DYNAMIC TORQUE CONTROL

In practice, a fast dynamic torque control can be achieved by fully utilizing a DC bus voltage through overmodulation strategy. The switching strategy to perform overmodulation mode during torque transient condition is usually referred to as dynamic overmodulation. In DTC-SVM, dynamic overmodulation occurs whenever there is a large torque demand such that the generated voltage reference vector exceeds the hexagonal boundary on a voltage vector plane. In hysteresis-based DTC, there is no voltage reference vector involved. However, an equivalent condition occurs whenever the hysteresis torque comparator produces a demand to continuously increase the torque. At the same time the flux is regulated to follow the circular path using two active voltage vectors.

A. Previous methods used for dynamic overmodulation

It had been reported that the overmodulation strategy is commonly utilized in space vector modulation (SVM) approach [23],[29]-[31],[35],[36]. For advanced motor control, the use of SVM is preferable than the other techniques (for example, [37][38] use triangular carrier based) since it is more flexible (uses only single reference voltage as the input modulator) and able to exploit the overmodulation region to six-step mode [23][31][36]. However, motor control performance using SVM is dependent on the accuracy of the estimation of the reference voltage. Moreover, the computations of reference voltage and maximum possible voltage used for the implementation of dynamic overmodulation leads to a more complex control structures. Several methods of dynamic overmodulation methods are reported. Fig. 3 compares some modified voltage references, $\mathbf{v_{[i]}}$ (e.g. when i =1, proposed in [1]) with respect to the original voltage reference vector, $\mathbf{v_{s,ref}}$, which is beyond the hexagonal boundary of the voltage vectors. Note that, voltage vector components are not drawn to scale. It can be seen that (from Fig. 1), [31] and [34] switched only single voltage vector which is $\mathbf{v_{k+2}}$ during dynamic overmodulation. This single selection of vector shows the occurrence of a six-step operation that produces the fastest dynamic torque control as will be discussed later in the paper. While the other methods result in slower dynamic torque response since two active states are alternately switched during the dynamic condition. For example, [29] used two active states utilizing dead-beat control in order to maintain the magnitude of stator flux under control for any condition.

Later, [30] was proposed to simplify the complexity control structure in [29], (where it does not provide a dead beat control of the magnitude flux as a transient torque encountered) and hence results in a faster dynamic torque control. In this way, the modified voltage vector, $\mathbf{v_{[30]}}$ has the same angle, γ as the original reference voltage, $\mathbf{v_{s,ref}}$ but with a modified magnitude. In [32], the reference voltage, $\mathbf{v_{s,ref}}$ was modified to $\mathbf{v_{[32]}}$ such that the error between the magnitude of $\mathbf{v_{[32]}}$ and $\mathbf{v_{s,ref}}$ is minimized. This means the modified voltage vector, $\mathbf{v_{[32]}}$ should be closest to the original reference vector $\mathbf{v_{s,ref}}$ by ensuring that a line joining the $\mathbf{v_{s,ref}}$ and $\mathbf{v_{[32]}}$ is orthogonal to the hexagon boundary.

Although the SVM technique has been widely used in many advanced DTC and field oriented control of motor drives, it actually complicates the original control and structure of the drive system. This is due to the fact that, more computation involving estimation of $\mathbf{v_{s,ref}}$ and approximation of modified voltage reference are required as mentioned above. The simplicity advantage of DTC hysteresis-based structure is lost.

B. Dynamic torque control in basic hysteresis-based DTC

It is well known that, the original DTC scheme proposed by Takahashi [1] offers fast instantaneous torque and flux control due to the optimized voltage vectors selection in controlling simultaneously both flux and torque. During large torque demand, hence large torque error, the hysteresis torque comparator produces a single status that requires an increase in torque. This means that under this condition, no zero vectors are selected to reduce the torque. At the same time, the flux hysteresis will regulate the flux to follow the circular path using two active voltage vectors. This is similar to a condition in DTC-SVM in which stator voltage reference vector follows the hexagonal boundary in overmodulation mode, which is the reference voltage $\mathbf{v_{[29]}}$ in Fig. 3. Since no zero voltage vectors are applied, rapid changes in the flux vector position and hence a quick dynamic torque response is achieved. However,

this method does not give the fastest dynamic torque response simply because two active voltage vectors are switched during dynamic condition. In order to achieve the fastest dynamic torque response only a single vector should be switched and held instead of two active voltage vectors.

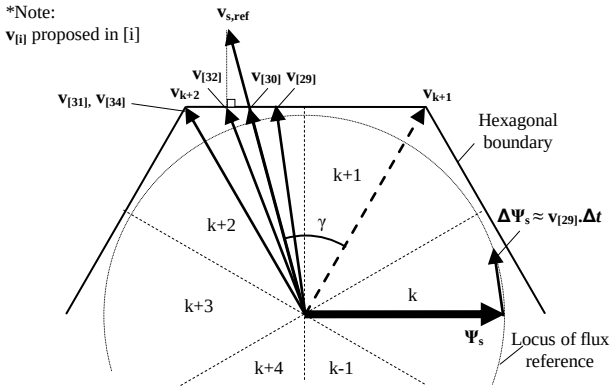

Fig. 3. Variations of proposed voltage vectors applied during dynamic overmodulation mode.

For the purpose of studying the effect of voltage vectors on the torque in DTC hysteresis-based drives, the torque equation will be expressed in terms of the stator flux and rotor flux magnitudes as given in (9).

$$T_e = \frac{3}{2} P \frac{L_m}{\sigma L_s L_r} \psi_s \psi_r \sin\delta_{sr} , \qquad (9)$$

where σ is the total leakage factor and δ_{sr} is the angle difference between the stator flux and rotor flux vectors and plays a vital role in controlling output torque. The relationship between the rotor flux vector and the stator flux vector in the rotor flux reference frame can be written as:

$$\boldsymbol{\Psi}_\mathbf{r}^\mathbf{r} = \frac{L_m / L_s}{1 + p\sigma\tau_r} \boldsymbol{\Psi}_\mathbf{s}^\mathbf{r} \qquad (10)$$

where τ_r is the rotor time constant. If the ohmic drop in equation (1) is neglected, then we can approximate the change in stator flux as

$$\Delta\boldsymbol{\Psi}_\mathbf{s} = \mathbf{v}_\mathbf{s} \Delta t \qquad (11)$$

Equation (11) indicates that an instantaneous angular velocity of the stator flux is irregular due to the switching voltage vectors. According to (10), the rotor flux will follow the stator flux, however with the irregular motion removed due to the low pass filtering action.

Fig. 4 shows the space vectors of the stator flux and rotor flux linkages moving in the counterclockwise direction. The motion of the stator flux is dictated by the voltage vectors $\mathbf{v_{k+1}}$ and $\mathbf{v_{k+2}}$. Case 1 is when the stator flux is about to enter sector k (at α_k = 0 rad.) while case 2 is when the stator flux is about to leave sector k (at α_k = π/3 rad.). The dynamic torque response can be studied by looking at the effects of applying the possible two voltage vectors on the angle $\Delta\delta_{sr}$. For this purpose, the vectors are redrawn as shown in Fig. 4(b). From Fig. 4(a) and (b), it can be seen that $\mathbf{v_{k+1}}$ has a larger tangential component to the circular flux locus while the component of $\mathbf{v_{k+2}}$ has a larger radial (negative) component in case 1. On the other hand, $\mathbf{v_{k+1}}$ has a larger radial component while $\mathbf{v_{k+2}}$ has a larger tangential component to the circular flux locus in case 2. Fig. 4(b) highlights the effect of selecting different switching states on $\Delta\delta_{sr}$. Based on the continuous rotation of the rotor flux as compared to the irregular rotation of stator flux, it can be seen that $\Delta\delta_{sr,1}$ is larger when $\mathbf{v_{k+1}}$ is switched for case 1 and on the other hand, $\Delta\delta_{sr,2}$ is larger when $\mathbf{v_{k+2}}$ is switched for case 2. In fact, if the sector is subdivided into subsectors, (i) and (ii) based on (12), vector $\mathbf{v_{k+1}}$ will result in a larger $\Delta\delta_{sr}$ throughout subsector (i) and $\mathbf{v_{k+2}}$ will give a larger $\Delta\delta_{sr}$ throughout subsector (ii).

$$\begin{aligned} &0 \le \alpha_k < \pi/6 \text{ rad.} \quad \text{for subsector i} \\ &\pi/6 \le \alpha_k < \pi/3 \text{ rad.} \quad \text{for subsector ii} \end{aligned} \qquad (12)$$

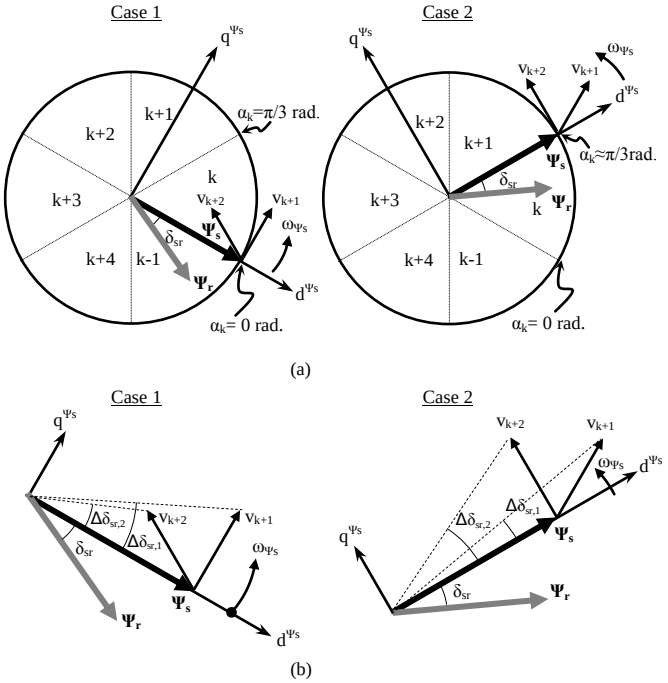

Fig. 4. Effects of selecting different switching under dynamic condition. (a) stator voltage vector in stator flux (b) comparison of the load angle, δ_{sr} generated by the same magnitude of appropriate voltage vectors.

According to (9), with a larger $\Delta\delta_{sr}$, $\mathbf{v_{k+1}}$ and $\mathbf{v_{k+2}}$ will give a faster dynamic torque response in the subsector (i) and (ii) respectively.

C. Proposed Dynamic torque control

In the proposed dynamic overmodulation method, the most optimized voltage vector that produce the largest tangential to the circular flux locus, is switched and held (instead of selecting two active voltage vectors) during torque dynamic to achieve the fastest dynamic torque control. As discuss in the

previous section, if sector k^{th} is considered, this would be vector $\mathbf{v_{k+1}}$ in subsector (i) and vector $\mathbf{v_{k+2}}$ in subsector (ii). Fig. 5 shows the structure of DTC-hysteresis based induction machine with the proposed modification of flux error status. Notice that all components of the DTC hysteresis-based scheme are retained, except for the inclusion of the 'modification of flux error status' block which is responsible to perform the dynamic overmodulation mode. The selection of the optimized voltage vector to give the fastest torque response can be simply done by modifying the flux error status (Ψ^+) to a new flux status (Ψ^-) before it is being fed to the look-up table. The 'modification of flux error status' block and hence the proposed dynamic overmodulation, is activated when the torque error E_{Te} is greater than twice of the hysteresis band of torque controller, HB_{Te}.

When the 'modification of flux error status' block is activated, the output of this block Ψ_s^- depends on the position of the flux position within a sector as shown in Fig. 6. If it is in subsector (i), $\Psi_s^- = 0$ hence $\mathbf{v_{k+1}}$ is selected and if it is in subsector (ii) $\Psi_s^- = 1$, $\mathbf{v_{k+2}}$ is selected. The border of the sectors and subsectors can be easily calculated using the threshold values of $\Psi_{s,q}{}^s$, denoted as $\Psi_{sq,1}$ and $\Psi_{sq,2}$, which can be calculated as

$$\Psi_{sq,1} = \Psi_{s,d}{}^s \tan(\pi/6) \quad (13)$$

$$\Psi_{sq,2} = \Psi_{s,d}{}^s \tan(\pi/3) \quad (14)$$

IV. Simulation and Experimental Results

To study on the effectiveness of the proposed dynamic overmodulation method, a simulation of the DTC hysteresis-based induction motor drive is performed using Matlab/Simulink simulation package. The parameters for the DTC drive and the actual parameters of an induction motor are as shown in Table II. To verify the feasibility of the proposed dynamic overmodulation scheme, a complete drive system as shown in Fig. 7 has been realized. The experimental set-up consists of an IGBT inverter and a 1.5 kW, four-pole squirrel cage induction motor. The DTC hysteresis-based system and induction machine parameters are same to the parameters used for the simulation. For safety reason, the DC voltage was limited to 240V, which means that the based speed is reduced to 570 rpm. It should be noted that using a higher DC voltage would further enhance the torque response since higher DC voltage will result in a higher rate of change of torque.

The control algorithm is implemented on a DSPACE 1102 and Altera FPGA (APEX20KE). The sampling period of the DTC scheme, including the proposed dynamic overmodulation is 55 μs.

Some tests have been carried out to compare the performance of dynamic torque control in the basic DTC hysteresis-based with and without the proposed dynamic overmodulation. For the sake of identification, the DTC without the proposed overmodulation is referred as DTC1, while the one with the proposed dynamic overmodulation strategy is referred as DTC2. The dynamic torque control is performed by applying a step change of torque reference from 1.5Nm to 9.0Nm at two different stator flux positions.

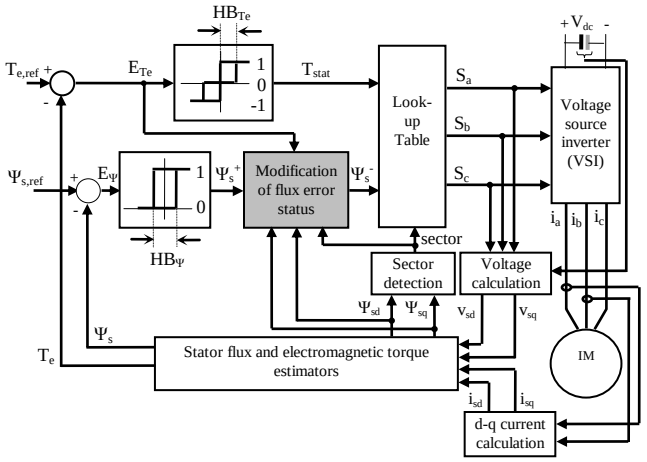

Fig. 5. Structure of DTC-hysteresis based induction machine with the proposed modification of flux error status block.

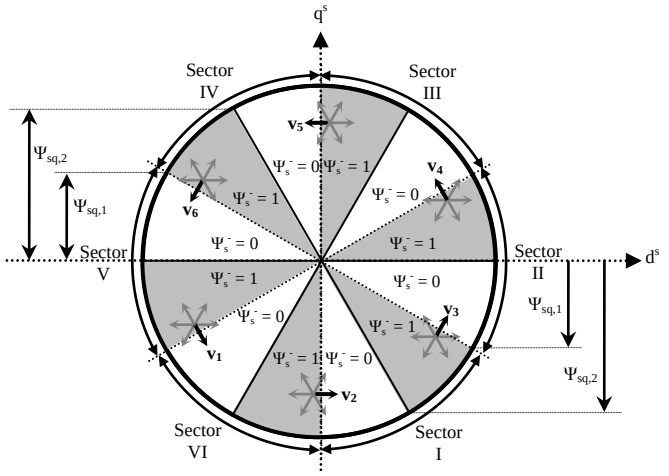

Fig. 6. The proposed digital outputs in modified flux error status correspond to the optimized voltage vectors for every subsector in each sector.

TABLE II
DTC-Hysteresis Based System and Induction Machine Parameters

Induction machine	
Rated power	1.5 kW
Rated voltage	400 V
Rated current	3.39 A
Rated speed	1410 rpm
Rated torque	9 Nm
Rated flux	0.892 Wb
Stator resistance	5.5 Ω
Rotor resistance	4.51 Ω
Stator self inductance	306.5 mH
Rotor self inductance	306.5 mH
Mutual inductance	291.9 mH
Number of poles	4
DTC-Hysteresis based System	
Flux hysteresis band, HB_Ψ	0.045 Wb
Torque hysteresis band, HB_{Te}	0.9 Nm
DC link voltage, V_{dc}	240 V

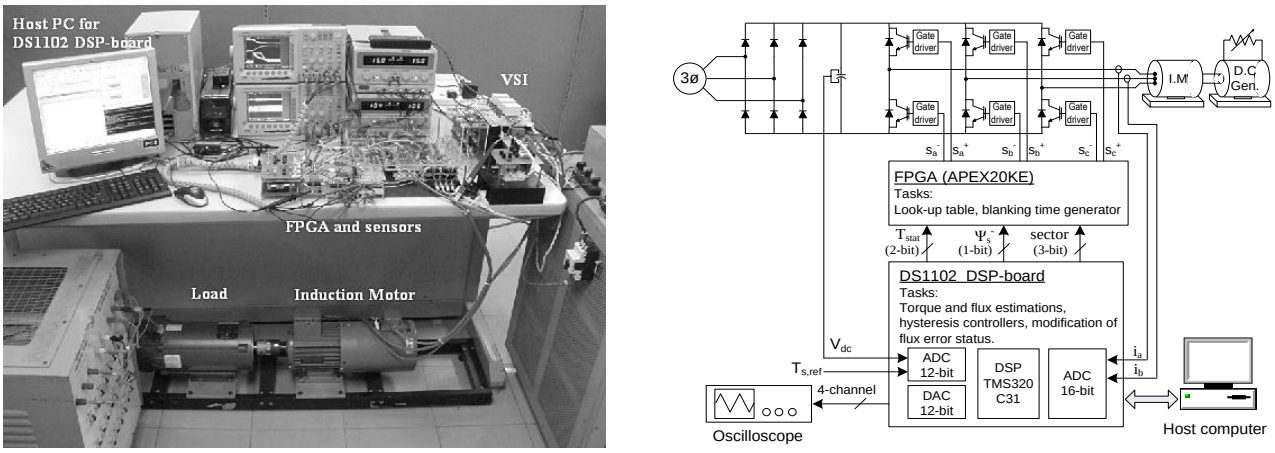

Fig. 7. Complete drive system (a) Picture of the experiment set-up, (b) functional block diagram of the experiment set-up

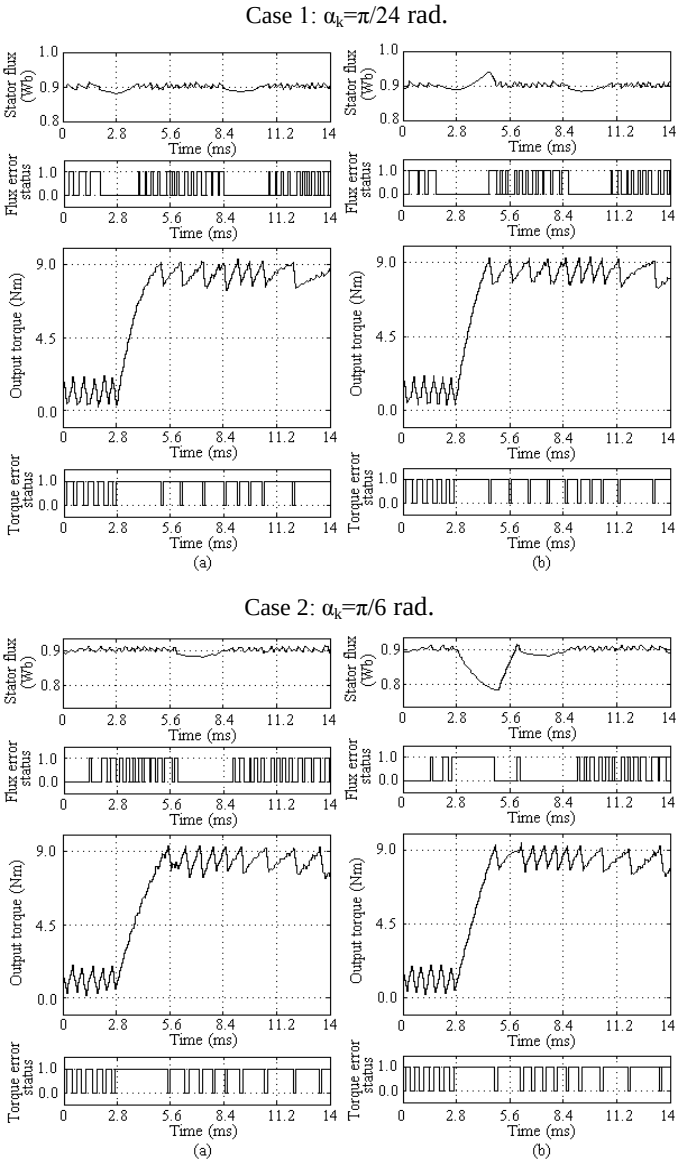

Fig. 8. Comparison by simulation of dynamic torque performance between (a) DTC1 and (b) DTC2, when a dynamic torque control occurs as the stator flux position at $\alpha_k=\pi/24$ rad. or $\alpha_k=\pi/6$ rad (at the middle of sector 2).

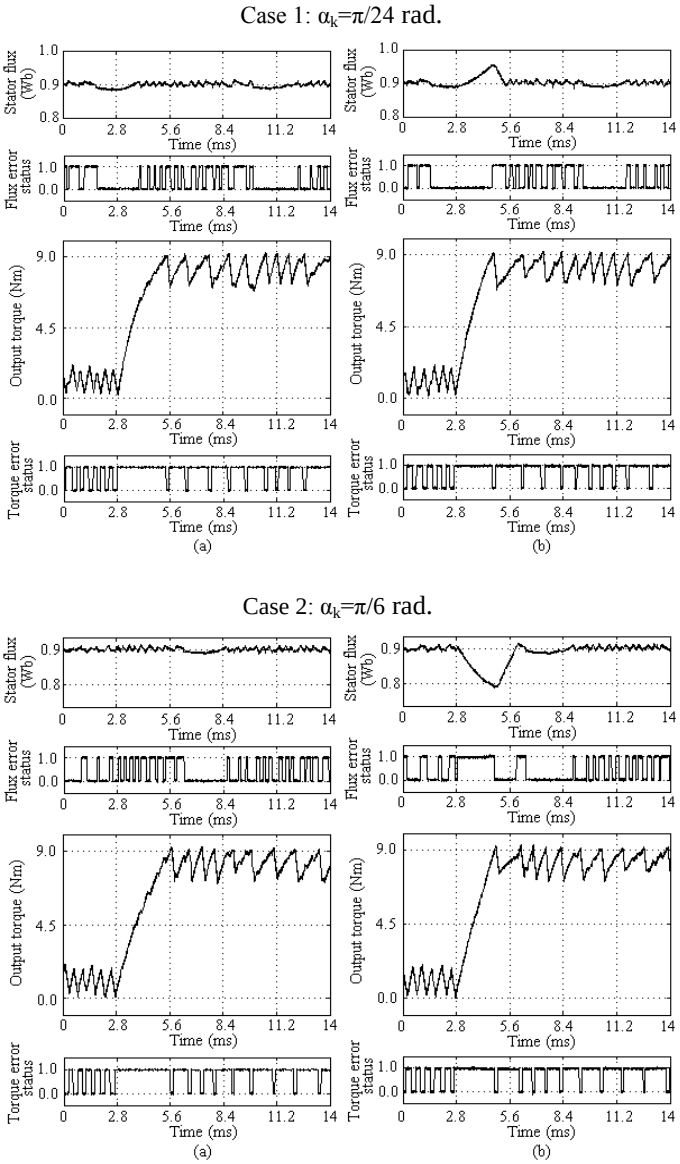

Fig. 9. Comparison by experimental of dynamic torque performance between (a) DTC1 and (b) DTC2, when a dynamic torque control occurs as the stator flux position at $\alpha_k=\pi/24$ rad. or $\alpha_k=\pi/6$ rad (at the middle of sector 2).

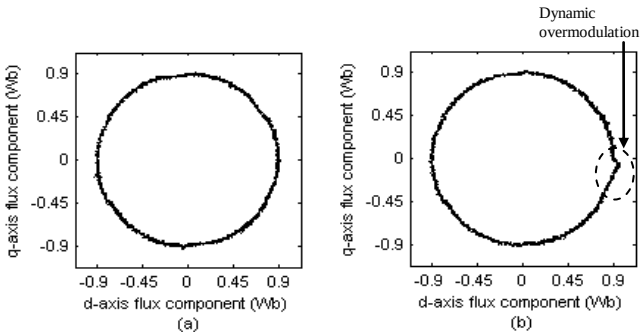

Fig. 10. Comparison of stator flux locus obtained in (a) DTC1 and (b) DTC2 (for one complete flux wave cycle) when a dynamic torque condition occurs at $\alpha_k=\pi/24$ rad.

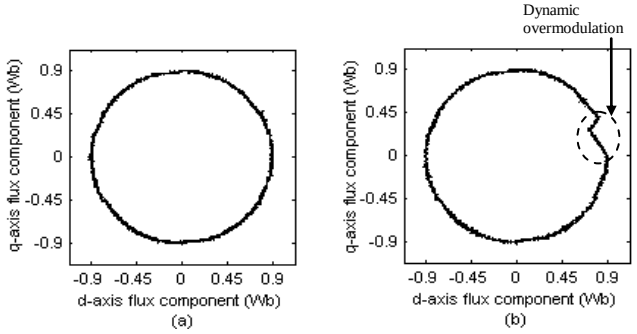

Fig. 11. Comparison of stator flux locus obtained in (a) DTC1 and (b) DTC2 (for one complete flux wave cycle) when a dynamic torque condition occurs at $\alpha_k=\pi/6$ rad.

Based on ψ_d^s and ψ_q^s, a step change in the torque reference is introduced at $\alpha_k=\pi/24$ rad. (subsector (i) within sector 2) and at $\alpha_k= \pi/6$ rad. (subsector (ii) within sector 2). To make the comparisons fair, the dynamic torque control in both DTC schemes were performed under the same load torque condition so that the rotor speed operated at around 410 rpm.

The simulation and experimental results under these two conditions are shown in Fig. 8 and Fig. 9, respectively. It can be seen that for DTC1, two active voltage vectors are selected during the torque dynamic; this is indicated by the flux error status waveform which switches between 1 and 0. For the proposed overmodulation (DTC2), single flux error status is held hence only single vector is selected during the torque dynamic. The selected voltage vector, as discussed in the previous section, provides the fastest torque response. The effect of the proposed overmodulation on the stator flux locus for the two different stator flux positions can be seen from the experimental results as shown in Fig. 10 and Fig. 11.

The shape and hence the magnitude of the stator flux are affected since single voltage vector is switched during the dynamic overmodulation. When the torque dynamic occurs in subsector (i), single voltage vector that produces the fastest

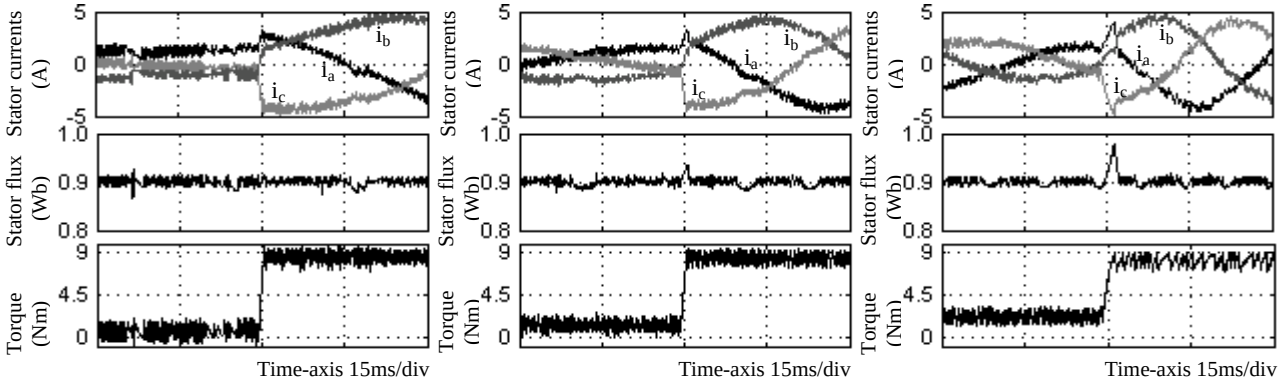

Fig. 12. The behavior of motor currents when the flux magnitude suddenly increases due to the proposed switching strategy as the dynamic torque occurs at $\alpha_k=\pi/24$ rad. The dynamic torque control is applied at three different speed operations for (a) Speed 1 at 100 rpm (b) Speed 2 at 300 rpm (c) Speed 3 at 550 rpm.

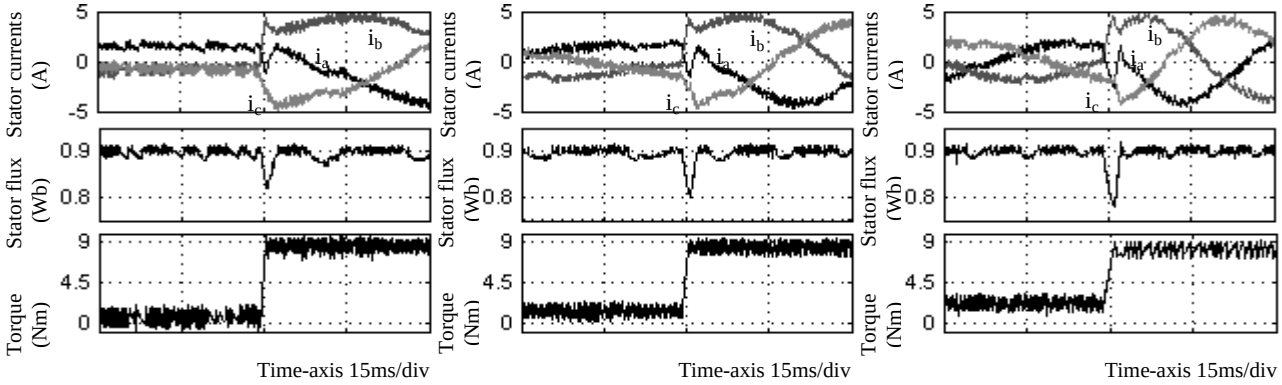

Fig. 13. The behavior of motor currents when the flux magnitude suddenly increases due to the proposed switching strategy as the dynamic torque occurs at $\alpha_k=\pi/6$ rad. The dynamic torque control is applied at three different speed operations for (a) Speed 1 at 100 rpm (b)Speed 2 at 300 rpm (c) Speed 3 at 550 rpm.

torque response is selected. This vector also increases the flux causing the flux locus to deviate from the circular locus momentarily as shown in Fig. 10. On the other hand, when the torque dynamic occurs in subsector (ii), a single voltage vector that gives the fastest torque response and at the same time reduces the flux is selected. This is indicated by the stator flux locus shown in Fig. 11. For both cases, the deviation in the flux locus from the circular locus occurs momentarily during the torque dynamic.

It is quite interesting to observe the behavior of motor currents as the flux magnitude is suddenly distorted due to the proposed switching strategy during torque dynamic condition. Figs. 12 and 13 highlight the behavior of motor currents for DTC2 at 3 different operating speeds named as Speed 1 (at 100 rpm), Speed 2 (at 300 rpm) and Speed 3 (at 550 rpm). These speeds represent 'low', 'medium' and 'high' speed ranges respectively, relative to the reduced based speed of 570rpm. For each operating speed, a step change of reference torque is applied at $\alpha_k=\pi/24$ rad. and $\alpha_k=\pi/6$ rad. As can be seen from the figures, the three-phase stator currents show rapid change during torque dynamic which occur in a relatively very short period especially for Speed 1. Thus, the possibility of facing over-current problem is not serious as the sharp increases of currents occur within a very short period of time. It can also be noticed that (in Figs. 12 and 13), the performance of dynamic torque control decreases (i.e produces slower torque response) as the motor speed operation increases. This is due to the fact that the rate of change of torque depends on operating conditions (i.e DC voltage, load torque, speed) which has been discussed in [39][40]. Nevertheless, regardless of the speed of operation, the torque response with the proposed dynamic overmodulation would give faster torque response when compared with the conventional DTC that use two voltage vectors during torque dynamic.

V. Conclusion

A simple dynamic overmodulation to achieve the fastest dynamic torque response in DTC hysteresis-based induction machine is proposed. An optimized voltage vector that produces the largest tangential to the circular flux locus is switched and held so that a fast rate of change of angle, $\Delta\delta_{sr}$ is achieved. The selection of the optimized voltage vector is simply obtained by modifying the flux error status before it is being fed to the look-up table. The main benefit of the proposed method is its simplicity and at the same time be able to produce the fastest dynamic torque response with six-step mode. The dynamic overmodulation is achieved without the need of space vector modulator.

Acknowledgment

The authors would like to thank the Ministry of Science, Technology and Innovation (MOSTI) of the Malaysian government for providing the funding for this research.

References

[1] Takahashi I, Naguchi T, "A new quick-response and high efficiency control strategy of an induction motor," IEEE Trans. Industry Applications, vol. IA-22, no. 5, pp. 820–827, 1986.

[2] Y. S. Lai and J. H. Chen, "A new approach to direct torque control of induction motor drives for constant inverter switching frequency and torque ripple reduction," *IEEE Trans. Energy Conversion*, vol. 16, pp. 220–227, Sept. 2001.

[3] L. Romeral, A. Arias, E. Aldabas, M.G. Jayne, "Novel DTC scheme with fuzzy adaptive torque-ripple reduction," *IEEE Trans. on Industrial Electronics*, vol. 50, no. 3, pp. 487-492, June 2003.

[4] N.R.N. Idris, A.H.M. Yatim, "Direct torque control of induction machines with constant switching frequency and reduced torque ripple," *IEEE Trans. on Industrial Electronics*, vol. 51, no. 4, pp. 758-767, August 2004.

[5] V. Ambrozic, G.S. Buja, R. Menis, "Band-constrained technique for direct torque control of induction motor," *IEEE Trans. on Industrial Electronics*, vol. 51, no. 4, pp. 776- 784, August 2004.

[6] C. Lascu, I. Boldea, F. Blaabjerg, "Variable-structure direct torque control - a class of fast and robust controllers for induction machine drives," *IEEE Trans. on Industrial Electronics*, vol. 51, no. 4, pp. 785-792, August 2004.

[7] C. Lascu, A.M. Trzynadlowski, "A sensorless hybrid DTC drive for high-volume low-cost applications," *IEEE Trans. on Industrial Electronics*, vol. 51, no. 5, pp. 1048- 1055, Oct 2004.

[8] T. Geyer, G. Papafotiou, M. Morari, "Model Predictive Direct Torque Control-Part I: Concept, Algorithm, and Analysis," *IEEE Trans. on Industrial Electronics*, vol. 56, no. 6, pp. 1894-1905, June 2009.

[9] G. Papafotiou, J. Kley, K. G. Papadopoulos, P. Bohren, M. Morari, "Model Predictive Direct Torque Control—Part II: Implementation and Experimental Evaluation," *IEEE Trans. on Industrial Electronics*, vol. 56, no. 6, pp. 1906-1915, June 2009.

[10] J. Beerten, J. Verveckken, J. Driesen, "Predictive Direct Torque Control for Flux and Torque Ripple Reduction," *IEEE Trans. on Industrial Electronics*, vol. 57, no. 1, pp. 404-412, Jan 2010.

[11] Shyu, K.; Lin, J.; Pham, V.; Yang, M.; Wang, T., "Global Minimum Torque Ripple Design for Direct Torque Control of Induction Motor Drives," *IEEE Transactions on Industrial Electronics*, vol.57, no.9, pp.3148-3156, Sept. 2010.

[12] M. Cirrincione, M. Pucci, "An MRAS-based sensorless high-performance induction motor drive with a predictive adaptive model," *IEEE Trans. on Industrial Electronics*, vol. 52, no. 2, pp. 532- 551, April 2005.

[13] P. Correa, M. Pacas, J. Rodriguez, "Predictive Torque Control for Inverter-Fed Induction Machines," *IEEE Trans. on Industrial Electronics*, vol. 54, no. 2, pp. 1073-1079, April 2007.

[14] R. Morales-Caporal, M. Pacas, "A Predictive Torque Control for the Synchronous Reluctance Machine Taking Into Account the Magnetic Cross Saturation," *IEEE Trans. on Industrial Electronics*, vol. 54, no. 2, pp. 1161-1167, April 2007.

[15] M. Nemec, D. Nedeljkovic, V. Ambrozic, "Predictive Torque Control of Induction Machines Using Immediate Flux Control," *IEEE Trans. on Industrial Electronics*, vol. 54, no. 4, pp. 2009-2017, August 2007.

[16] H. Miranda, P. Cortes, J. I. Yuz, J. Rodriguez, "Predictive Torque Control of Induction Machines Based on State-Space Models," *IEEE Trans. on Industrial Electronics*, vol. 56, no. 6, pp. 1916-1924, June 2009.

[17] S. Bolognani, L. Peretti, M. Zigliotto, "Design and Implementation of Model Predictive Control for Electrical Motor Drives," *IEEE Trans. on Industrial Electronics*, vol. 56, no. 6, pp. 1925-1936, June 2009.

[18] F. Barrero, M. R. Arahal, R. Gregor, S. Toral, M. J. Duran, "A Proof of Concept Study of Predictive Current Control for VSI-Driven Asymmetrical Dual Three-Phase AC Machines," *IEEE Trans. on Industrial Electronics*, vol. 56, no. 6, pp. 1937-1954, June 2009.

[19] F. Barrero, M. R. Arahal, R. Gregor, S. Toral, M. J. Duran, "One-Step Modulation Predictive Current Control Method for the Asymmetrical Dual Three-Phase Induction Machine," *IEEE Trans. on Industrial Electronics*, vol. 56, no. 6, pp. 1974-1983, June 2009.

[20] F. Morel, X. Lin-Shi, J.-M. Retif, B. Allard, C. Buttay, "A Comparative Study of Predictive Current Control Schemes for a Permanent-Magnet Synchronous Machine Dr," *IEEE Trans. on Industrial Electronics*, vol. 56, no. 7, pp. 2715-2728, July 2009.

[21] M. Pacas, J. Weber, "Predictive direct torque control for the PM synchronous machine," *IEEE Trans. on Industrial Electronics*, vol. 52, no. 5, pp. 1350- 1356, Oct 2005.
[22] G. Foo, M. F. Rahman, "Sensorless Direct Torque and Flux-Controlled IPM Synchronous Motor Drive at Very Low Speed Without Signal Injection," *IEEE Trans. on Industrial Electronics*, vol. 57, no. 1, pp. 395-403, Jan 2010.
[23] A.M. Khambadkone, J. Holtz, "Compensated synchronous PI current controller in overmodulation range and six-step operation of space-vector-modulation-based vector-controlled drives," *IEEE Trans. on Industrial Electronics*, vol. 49, no. 3, pp. 574-580, June 2002.
[24] M. Fu and L. Xu, "A sensorless direct torque control technique for permanent magnet synchronous motors," in *Conf. Rec. IEEE-IAS Annu. Meeting*,vol. 1, 1999, pp. 159–164.
[25] D. Casadei, G. Serra, A. Tani, L. Zarri, and F. Profumo, "Performance analysis of a speed-sensorless induction motor drive based on a constant-switching-frequency DTC scheme," *IEEE Trans. Ind. Appl.*, vol. 39, no. 2, pp. 476–484, Mar./Apr. 2003.
[26] Y. Xue, X. Xu, T. G. Habetler, and D. M. Divan, "A low cost stator flux oriented source variable speed drive," in *Conf. Rec. 1990 IEEE-IAS Annu. Meeting*, 1990, vol. 1, pp. 410–415.
[27] C. Lascu, I. Boldea, and F. Blaabjerg, "A modified direct torque control for induction motor sensorless drive," *IEEE Trans. Ind. Applications*, vol. 36, pp. 122–130, Feb. 2000.
[28] F. Hoffmann and M. Janecke, "Fast Torque Control of an IGBT-Inverter Fed Three-Phase A.C. Drive in the Whole Speed Range – Experimental Results," in *6th European Power Electronic Conference*, (Sevilla, Spain), pp. 3.399–404, 1995.
[29] T. Habetler, F. Profumo, M. Pastorelli, L. Tolbert. "Direct Torque Control of Induction Machines Using Space Vector Modulation". IEEE Trans. on Industry Applications, 28(5):1045–1053, September/October 1992.
[30] T. G. Habetler, F. Profumo, and G. Griva, "Performance evaluation of a direct torque controlled drive in the continuous PWM-square wave transition region," IEEE Trans. Power Electron., vol. 10, no. 4, pp. 464- 471, 1995.
[31] Tripathi, A. M. Khambadkone, S.K. Panda, "Dynamic Control of Torque in Overmodulation and in the Field weakening region," IEEE Transactions on Power Electronics, vol. 21, No. 4, pp. 1091-1098, July 2006.
[32] H. Mochikawa, T. Hirose, and T. Umemoto, "Overmodulation of voltage source pwm inverter," in Proc. JIEE Int. Soc. Conf., 1991, pp. 466–471.
[33] S. Jul-Ki and S. K. Sul, "A new overmodulation strategy for induction motor drive using space vector pwm," in *Proc. IEEE Appl. Power Electron. Conf.*, Mar. 1995, pp. 211–216.
[34] M. Depenbrock, "Direct Self Control of inverter-fed of induction machine , IEEE Trans. Power Electron., vol3,pp. 420-429, 1988.
[35] DW Chung and SK Sul, "A new dynamic overmodulation strategy for high performance torque control of induction motor drives", 14th Applied Power Electronics Conference and Exposition (APEC 99), Vol 1, pp 264-270, 1999.
[36] J. Holtz, W. Lotzkat, and A. Khambadkone, "On continuous control of pwm inverters in the overmodulation range including the six-step mode," IEEE Trans. on Power Electronics, vol. 8, no. 5, pp. 546–553, Oct. 1993.
[37] A. M. Hava, S.-K. Sul, R. J. Kerkman, and T. A. Lipo, "Dynamic overmodulation characteristics of triangle intersection pwm methods," *IEEE Trans. Ind. Appl.*, vol. 35, no. 4, pp. 896–907, Jul./Aug. 1999.
[38] R. J. Kerkman, T. M. Rowan, D. Leggate, and B. J. Seibel, "Control of pwm voltage inverters in pulse dropping range," *IEEE Ind. Appl. Mag.*, vol. 2, no. 5, pp. 24–31, Sep./Oct. 1996.
[39] D. Casadei, G. Serra, A. Tani, "Analytical investigation of torque and flux ripple in DTC schemes for induction motors," *Proc. IEEE-IECON'97,* New Orleans, pp. 552-556.
[40] J. W. Kang and S. K. Sul, "Analysis and prediction of inverter switching frequency in direct torque control of induction machine based on hysteresis bands and machine parameters," *IEEE Transactions on Industrial Electronics*, vol. 48, pp. 545-553, 2001.

Auzani Jidin (S'09 IEEE) received his B.Eng. degree and M.Eng. degree in Power Electronics & Drives from Universiti Teknologi Malaysia (UTM), Malaysia in 2002 and 2004, respectively and currently PhD Student in the same University.

He is a lecturer in Department of Power Electronics and Drives, Faculty of Electrical Engineering at Universiti Teknikal Melaka Malaysia (UTeM), Malaysia. His research interests include the field of power electronics, motor drive systems, FPGA and DSP applications.

Nik Rumzi Nik Idris (M'97–SM'03) received the B.Eng. degree in Electrical Engineering from the University of Wollongong, Australia, the M.Sc. degree in power electronics from Bradford University, West Yorkshire, U.K., and the Ph.D. degree from Universiti Teknologi Malaysia (UTM) in 1989, 1993, and 2000, respectively.

He is an Associate Professor at the Universiti Teknologi Malaysia, and an Administrative Committee Member of the Industry Applications Societies/Power Electronics/Industrial Electronics Joint Chapter of IEEE Malaysia Section. His research interests include ac drive systems and DSP applications in power electronic systems.

Abdul Halim Mohamed Yatim (M'89–SM'01) received the B.Sc. degree in electrical and electronic engineering from Portsmouth Polytechnic, U.K., in 1981, and the M.Sc. and Ph.D. degrees in power electronics from Bradford University, U.K., in 1984 and 1990, respectively.

He is a Professor at the Universiti Teknologi Malaysia and Dean of the Faculty. Dr. Yatim is a Corporate Member of the Institution of Engineers Malaysia. He is a Registered Professional Engineer with the Malaysian Board of Engineers. He currently holds the Interim Chapter Chair of the Malaysian Section of the IEEE Industrial Electronics/Industry Applications/Power Electronics Joint Societies.

Tole Sutikno (S'08 IEEE) received his B.Eng. and M.Eng. degree in Electrical Engineering from Diponegoro University, Indonesia and Gadjah Mada University, Indonesia, in 1999 and 2004, respectively. Since 2001 he has been a lecturer in Electrical Engineering Department, Universitas Ahmad Dahlan (UAD), Indonesia. Currently, he is pursuing PhD degree at the Universiti Teknologi Malaysia (UTM), Malaysia. His research interests include the field of power electronics, motor drive systems and FPGA applications.

Malik E. Elbuluk (S'79–M'79–SM'97) received the B.Sc. (with honors) degree from University of Khartoum, Sudan, and the M.S., E.E., and D.Sc. degrees from Massachusetts Institute of Technology, Cambridge, in 1976, 1980, 1981, and 1986, respectively, all in Electrical Engineering.
He is a Professor at the University of Akron, Akron, OH, where he has been since 1989. His teaching and research interests include the areas of power electronics, electric machines, control systems, fuzzy logic, and neural networks.

Prof. Elbuluk actively publishes and reviews papers for IEEE Conferences and Transactions, and has organized and chaired a number of sessions for the PE, the IA and the IE Societies. He was an Associate Editor for the IEEE Transactions on PE and Vice President for the IEEE Transactions on IA and for the IACC. He is a Registered Professional Engineer in the State of Ohio.